

# Theoretical insight into adenine-uracil and adenine-thymine photodeactivation mechanisms.

Kinga Szkaradek,<sup>\*,a</sup> and Robert W. Góra,<sup>\*,a</sup>

Received Date

Accepted Date

DOI: 10.1039/xxxxxxxxxx

www.rsc.org/journalname

In this work, a thorough description of the photochemical and photophysical response of the Watson–Crick base pairs of adenine with uracil (A-U) or thymine (A-T) according to the SCS-ADC(2) results is discussed. Although widely explored, these systems lack a complete characterization of possible intra- and intermolecular relaxation channels induced by charge- or proton-transfer phenomena that may result due to the interaction of nucleobases in electronically excited states. In particular, we address the still open debate on photodeactivation via purine-ring puckering at the C2 or C6-atom position. We also consider the presence of low-lying long-living  $^1n\pi^*$  states to be a significant factor in the relaxation handicap through the EDPT process, as population of these states leads to internal conversion processes or efficient intersystem crossing to triplet manifold, whose estimated rate of  $1.6 \times 10^{10} \text{ s}^{-1}$ , exceeds by an order of magnitude the corresponding internal conversion to the ground state. Additionally, the use of the SCS variant of the ADC(2) method is shown to provide a more balanced description of valence and charge-transfer excited states.

## 1 Introduction

The photochemical and photophysical properties of nucleobases have been studied for decades.<sup>1–8</sup> Although widely explored, these systems continue to be an important subject of scientific curiosity due to the wide range of photodeactivation mechanisms under UV exposure and discrepancies regarding their mechanistic details.<sup>5–7</sup> The situation becomes much more complex in nucleic acids, where additional processes may occur, including the formation of delocalized excitonic and excimeric states, excitation energy transfer, intrastrand and interstrand electron and proton transfer processes, among others.<sup>7,8</sup> In general, in aggregates of nucleobases, the local *intramolecular* nonradiative decay processes compete with *intermolecular* processes, and the simplest model systems to study these processes are hydrogen-bonded or stacked nucleobase dimers.<sup>9–29</sup>

Surprisingly, studies of these processes on an equal footing are scarce, even for canonical base pairs. Theoretical studies of base pairs generally focus on plausible intermolecular processes, in particular electron-driven proton transfer (EDPT),<sup>9,30</sup> which is agreed to be the main deactivation channel of the photoexcited gas-phase Watson–Crick (WC) guanine-cytosine (G-C) base pair. It is firmly established that in this system, the population of the dark  $^1\pi_G\pi_C^*$  charge-transfer (CT) state, associated with a significant electron density transfer from the purine to the pyrimidine, leads to a very efficient photoexcitation decay within

$\sim 100 \text{ fs}$ ,<sup>9,11,31,32</sup> which causes a characteristic broad UV absorption band in the gas phase.<sup>31</sup> The most likely mechanistic explanation of this process is the transfer of a proton from the N1 atom of guanine to the N3 atom of cytosine, which stabilizes the CT state and eventually leads to a crossing with the ground state in a barrierless manner.<sup>7,9,23,33</sup>

Although a direct photoinduced EDPT process is unlikely in DNA,<sup>20</sup> there are spectroscopic indications that it could be possible within the A-U pair in the A-form RNA double helix.<sup>34</sup> The photochemistry of adenine complexes with uracil (A-U) or thymine (A-T) has received less attention than G-C,<sup>10,13,15,16,27,35</sup> and these have been studied mainly in the context of the plausibility of the spurious EDPT deactivation mechanism. Given the apparent similarities of uracil and thymine<sup>34,36–38</sup> and according to *ab initio* calculations, this mechanism should be possible in the WC base pair of A-T.<sup>10,16,23,39</sup> However, its experimental verification was hindered due to a different equilibrium geometry assumed in the gas phase.<sup>40,41</sup> Also, recent computational results of Jouybari et al.<sup>27</sup> did not yield the population of the CT state in nonadiabatic dynamics, which in this system is too far apart from the optically accessible locally excited (LE) state in the Franck–Condon region. Instead, the authors suggest that the main decay path of A-T involves a LE  $^1\pi\pi^*$  transition on the thymine, which is consistent with the experimental findings. Femtosecond pump-probe ionization spectroscopy of A-T vapors indicates that after excitation to the lowest  $^1\pi\pi^*$  state, internal conversion leads to the population of the  $^1n\pi^*$  state having a lower energy, with a lifetime of 2.4 ps.<sup>42</sup> In a subsequent study of Samoylova et al.<sup>13</sup> an additional decay channel was observed with a lifetime of approximately 40 ps that was tentatively assigned to an intermolecular relaxation process.

<sup>a</sup> Institute of Advanced Materials, Wrocław University of Science and Technology, Faculty of Chemistry, Wybrzeże Wyspiańskiego 27, 50-370, Wrocław, Poland; E-mail: robert.gora@pwr.edu.pl

† Electronic Supplementary Information (ESI) available: conformational analysis, selected excitation energies, spin-orbit couplings, results of transition rate calculations and a scheme of deactivation mechanisms for the A-T WC base pair. See DOI: 10.1016/b000000x/

In this work, we attempt to provide credible insight into plausible intra- and intermolecular photoinduced processes in the A-U and A-T WC base pairs. Although the photodynamics of isolated nucleobases is well known and there have been earlier attempts to describe the mechanism of photoinduced hydrogen transfer in canonical nucleobase pairs, the deactivation of the A-U and A-T base pairs through intramolecular channels has not been thoroughly studied.

## 2 Methods

The equilibrium geometries of the ground state were located using the second-order Møller–Plesset perturbation theory (MP2).<sup>43</sup> The relevant stationary points on the excited-state potential energy (PE) surfaces and the minimum energy crossing points (MECPs) of the adiabatic PE surfaces were found using the spin component scaling variants<sup>44</sup> of Algebraic Diagrammatic Construction up to the second order (SCS-ADC(2))<sup>45,46</sup> or SCS-MP2 methods for the excited and ground electronic states, respectively. The vertical excitation energies and other excited-state properties were obtained using the SCS-ADC(2) method. In general, no symmetry constraints were imposed during geometry optimization. All of the above calculations were performed using the Turbomole 7.3 package<sup>47</sup> and assuming the cc-pVTZ correlation-consistent basis set.<sup>48</sup>

The relevant MECPs were located using the sequential penalty-constrained optimization proposed by Levine, Martnez, and Coe and implemented in the CIOpt package.<sup>49</sup> The potential energy profiles were computed by linear interpolation in internal coordinates (LIIC) between stationary points using the same electronic structure calculation methods, i.e., the SCS-MP2 and SCS-ADC(2) methods and the cc-pVTZ basis set. The reliability of the SCS-MP2/SCS-ADC(2) PE profiles was tested against the multiconfigurational second-order *n*-electron valence state perturbation theory (NEVPT2) results obtained assuming the state-averaged (SA) complete active space self-consistent field (CASSCF) reference wavefunction and cc-pVTZ basis set. The active space in NEVPT2 calculations included 10 electrons correlated in 8 orbitals (3 occupied  $\pi$ , 2 occupied *n* and 3 virtual  $\pi^*$ ) and was averaged over the two lowest-lying states.

The intermolecular charge transfer character of the electronic states was assigned based on the transition density matrix analysis proposed by Plasser et al.<sup>50</sup> The charge transfer numbers defined as partial summations over squared transition density matrix elements of molecular fragments were calculated using the TheoDore 1.5.1 package.<sup>50–52</sup> These numbers were computed based on the Mulliken type analysis<sup>53</sup> and were used to determine the weight of charge transfer configurations for a given state (denoted as  $\Omega_{CT}$ ). This quantity vanishes for localized or delocalized Frenkel excitonic states and approaches unity for charge transfer or charge resonance states.

The transition rates of radiative and nonradiative processes were calculated using the thermal vibration correlation function (TVCF) formalism for excited state decay, developed by Shuai et al.<sup>54–56</sup> and implemented in MOMAP 2020.B package.<sup>57</sup> Due to the availability of non-adiabatic coupling terms, these calculations were performed using the TD-DFT approach, assuming

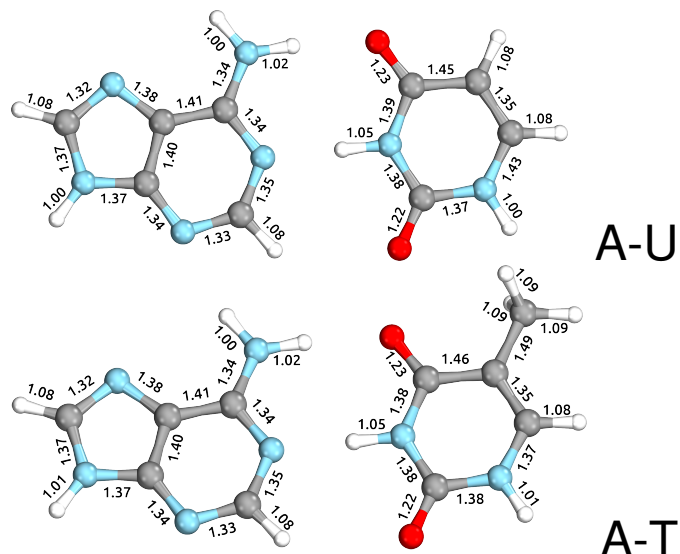


**Fig. 1** Geometries of canonical nucleobases paired in the Watson-Crick scheme, optimized at the MP2/cc-pVTZ level of theory.

$\omega$ B97X-D3 exchange-correlation functional and def2-SVP basis set available in the QChem 6.1 package.<sup>58</sup> Further details of these calculations are reported in the ESI.

## 3 Results and discussion

### 3.1 Electronic states in the Franck–Condon region

Equilibrium geometries of the canonical WC base pairs A-U and A-T are presented in Fig. 1 with the corresponding bond lengths. Geometry optimization without symmetry constraints generally yields planar or quasiplanar structures of heterocyclic rings with minor deviations owing to the pyramidalization of amino groups or the presence of a methyl group. In the ESI we also report other local minima of the A-U complexes located and the corresponding selected vertical excitation energies.

The located equilibrium geometries were assumed in consecutive single-point calculations of vertical excitation energies for 15 lowest-lying excited states. Table 1 presents vertical excitation energies for selected low-lying electronic states with corresponding oscillator strengths and assigned transition characters (the lower indices indicate the localization of a given orbital). The vertical spectra in the FC region are similar for both systems, with seemingly minor changes in the ordering of the corresponding excited states. In particular, in A-T the lowest-lying excited state of a  ${}^1\pi_T\pi_T^*$  character is located at 5.30 eV and is the  $S_3$  excited state, whereas the  ${}^1\pi_U\pi_U^*$  is the  $S_4$  excited state lying at 5.46 eV. However, this change may be significant considering the subsequent population of the lower-lying LE state of  ${}^1n\pi^*$  character and further relaxation on its hypersurface. The lowest lying  ${}^1n\pi^*$  state is located at about 5.1 eV in both systems and is associated with the electronic transition from the carbonyl oxygen lone electron pair to the  $\pi^*$  orbital localized on the aromatic ring of the respective pyrimidine.

It is interesting to note that the experimental results<sup>42</sup> regarding the A-T dimer indicate that after excitation to the lowest  ${}^1\pi\pi^*$  state, internal conversion leads to the population of the  ${}^1n\pi^*$  state

**Table 1** Properties of selected low-lying electronic states of canonical base pairs A-T and A-U, calculated using SCS-ADC(2)/cc-pVTZ method assuming the ground-state equilibrium geometries optimized using MP2/cc-pVTZ method. The oscillator strengths ( $f_{\text{osc}}$ ), vertical excitation energies in eV ( $E_{\text{exc}}$ ) and the weights of the CT configurations ( $\Omega_{\text{CT}}$ ) are reported. The last column shows the reference values of excitation energies calculated at the EOM-CC level.<sup>a</sup>

| Base  | State/Transition   | $f_{\text{osc}}$   | $E_{\text{exc}}$      | $\Omega_{\text{CT}}$ | $E_{\text{exc}}^{\text{EOM-CC}}$ |  |
|---|--|--|-----------------------|----------------------|----------------------------------|--|
| A-T   | S <sub>1</sub> $n_{\text{T}}\pi_{\text{T}}^*$                                  | $5.334 \cdot 10^{-5}$  | 5.11                  | 0.050                | 5.24                             |  |
|   | S <sub>2</sub> $\pi_{\text{A}}\pi_{\text{A}}^*$                                | 0.015  | 5.19                  | 0.008                | 5.34                             |  |
|   | S <sub>3</sub> $\pi_{\text{T}}\pi_{\text{T}}^*/\pi_{\text{A}}\pi_{\text{A}}^*$ | 0.284  | 5.30                  | 0.012                | 5.52                             |  |
|   | S <sub>4</sub> $\pi_{\text{A}}\pi_{\text{A}}^*/\pi_{\text{T}}\pi_{\text{T}}^*$ | 0.239  | 5.39                  | 0.009                | 5.60                             |  |
|   | S <sub>5</sub> $n_{\text{A}}\pi_{\text{A}}^*$                                  | $3.558 \cdot 10^{-4}$  | 5.64                  | 0.044                | 5.65                             |  |
|   | S <sub>9</sub> $\pi_{\text{A}}\pi_{\text{T}}^*$                                | 0.292  | 6.60                  | <b>0.428</b>         |                                  |  |
|   | S <sub>11</sub> $\pi_{\text{A}}\pi_{\text{T}}^*$                               | 0.238  | 6.66                  | <b>0.505</b>         |                                  |  |
|   | S <sub>13</sub> $n_{\text{T}}\pi_{\text{T}}^*$                                 | $1.569 \cdot 10^{-4}$  | 6.90                  | 0.102                |                                  |  |
|   | A-U  | S <sub>1</sub> $n_{\text{U}}\pi_{\text{U}}^*$                                  | $9.254 \cdot 10^{-5}$ | 5.09                 | 0.049                            |  |
|   |  | S <sub>2</sub> $\pi_{\text{A}}\pi_{\text{A}}^*$                                | 0.017                 | 5.19                 | 0.007                            |  |
|   |  | S <sub>3</sub> $\pi_{\text{A}}\pi_{\text{A}}^*/\pi_{\text{U}}\pi_{\text{U}}^*$ | 0.338                 | 5.33                 | 0.008                            |  |
|   |  | S <sub>4</sub> $\pi_{\text{U}}\pi_{\text{U}}^*/\pi_{\text{A}}\pi_{\text{A}}^*$ | 0.178                 | 5.46                 | 0.009                            |  |
|   |  | S <sub>5</sub> $n_{\text{A}}\pi_{\text{A}}^*$                                  | $3.288 \cdot 10^{-4}$ | 5.65                 | 0.041                            |  |
| S <sub>9</sub> $\pi_{\text{A}}\pi_{\text{U}}^*$                                 |  | 0.152  | 6.57                  | <b>0.659</b>         |                                  |  |
| S <sub>11</sub> $\pi_{\text{A}}\pi_{\text{A}}^*/\pi_{\text{A}}\pi_{\text{A}}^*$ |  | 0.373  | 6.65                  | <b>0.260</b>         |                                  |  |
| S <sub>14</sub> $n_{\text{U}}\pi_{\text{U}}^*$                                  |  | $1.638 \cdot 10^{-4}$  | 6.93                  | 0.137                |                                  |  |

<sup>a</sup> EOM-CCSD/cc-pVDZ results adopted from Benda et al.<sup>21</sup> for A-T in the arrangement denoted WW1.

having a lower energy, with a lifetime of 2.4 ps. The same study shows that the nonradiative transition from the  $^1\pi\pi^*$  to the  $^1n\pi^*$  state through a conical intersection occurs at an ultrafast pace < 100 fs (that assignment was based on Koopmans' ionization correlations calculated at the TD-B3LYP/6-31++G(d,p) level). The ordering of states and the position of  $n\pi^*$  states in the singlet manifold are particularly important because they lie below both the CT and the lowest bright state in the FC region, increasing the probability of their population in the photodynamics of A-T/A-U.

Recently, we discussed an alternative EDPT process that occurs on the  $^1n\pi_{\text{CT}}^*$  hypersurface of the guanine-cytosine (G-C) base pair.<sup>25</sup> However, the analysis of the natural transition orbitals revealed a minor weight of the charge transfer configurations for the lowest-lying  $^1n\pi^*$  states of A-U/A-T (denoted as  $\Omega_{\text{CT}}$  in Table 1). The partial CT character of  $^1n\pi^*$  excited states is observed only for higher-lying states (at about 6.9 eV). Therefore, we conclude that an analogous mechanism is not available from the FC region in the case of A-T and A-U base pairs. This may be one of the reasons why both thymine and uracil are more vulnerable to photodamage than cytosine in the nucleic acid duplex.<sup>59</sup>

Although  $^1n\pi^*$  states usually have very weak spectral features due to negligible oscillator strength, trapping a molecule for tens to hundreds of nanoseconds in such a dark reactive state could have significant consequences. Particularly interesting in this context is that  $^1n\pi^*$  states can contribute to both photostability and photodamage of nucleic acids due to their long-lived character and the possibility of a population of triplet states in pyrimidines through efficient ISC.<sup>60–63</sup>

As indicated in earlier studies, the charge transfer state of the  $^1\pi\pi^*$  character lies substantially higher than the bright state. According to our SCS-ADC(2) calculations the S<sub>9</sub> state is the lowest CT state located at 6.66 and 6.57 eV in the FC region, respectively, for A-T and A-U. This is more 1.1 eV above the bright state (cf. Table 1) and significantly higher than previous CC2 estimates reported by Perun et al. (6.26 eV)<sup>10</sup> and Benda et al. (6.29 eV).<sup>21</sup> We refer to the latter article for an extensive discussion of the earlier computational results. In general, CC2 calculations estimate the CT state at about 0.6–0.8 eV above the bright state in the FC region,<sup>21</sup> which compares well with the ADC(2) results (0.84 and 0.80 eV for A-T and A-U, respectively). However, the SCS scheme significantly destabilizes CT states,<sup>64</sup> thus bringing the SCS-ADC(2) results closer to the reference NEVPT2 values (see Fig. 6 in the **Calibration** section and the discussion thereof). Given that the population of the CT state can be challenging,<sup>7,27</sup> the excited-state dynamics of the studied base pairs is likely dominated by intramolecular processes. This conclusion is supported by transient electronic and vibrational absorption spectroscopies of the substituted A-T base pair.<sup>40</sup>

Therefore, A-T can decay through a local  $^1\pi\pi^*$  transition associated with purine puckering at the C2- or C6-atom position<sup>65</sup> or through processes involving  $^1\pi\pi^*$ <sup>27</sup> and  $^1n\pi^*$  transitions on pyrimidine.

Excitation decay through the EDPT channel in A-T/A-U WC base pairs appears unlikely or of secondary importance.<sup>27,40,66,67</sup> However, evidence of the EDPT decay channel involving H-bonded A-U base pairs that has a relatively short timescale of 2.9 ps,<sup>34</sup> which is virtually identical to that reported by Röttger et al.<sup>68</sup> for the WC base pair of G-C, calls for thorough theoretical investigation. These findings are rather unexpected considering also that a corresponding channel seems inaccessible in both the gas phase A-T and the double-stranded d(A)<sub>n</sub>-d(T)<sub>n</sub> duplex.<sup>20</sup> Given the apparent similarities of uracil and thymine, the same obstacles to detect EDPT should be assumed in the base pair A-U. Specifically, a negligible population of WC conformers in the gas phase (see ESI) and the influence of the RNA environment that was discussed in several studies.<sup>34,36–38</sup> Consequently, it remains interesting to investigate the EDPT process, particularly in WC A-U, compared to intramolecular radiationless deactivation mechanisms.

### Comparison of intra- and intermolecular deactivation mechanisms

The calculations started with optimization of the minima on the S<sub>1</sub> PE surfaces for A-T and A-U using the SCS-ADC(2)/cc-pVTZ method, initiated by forcing the transfer of a proton from adenine to thymine or uracil. The S<sub>1</sub>/S<sub>0</sub> energy gaps dropped below 1 eV at the located S<sub>1</sub> minima; therefore, these geometries provided an excellent starting point to determine the MECPs between the S<sub>1</sub> and S<sub>0</sub> PE surfaces. Considering that the  $^1n\pi^*$  dark LE state located on the pyrimidine moiety is the lowest lying singlet state for the A-U and A-T systems, a subsequent MECP optimization was performed in search of the photorelaxation channel on the  $^1n\pi^*$  hypersurface.

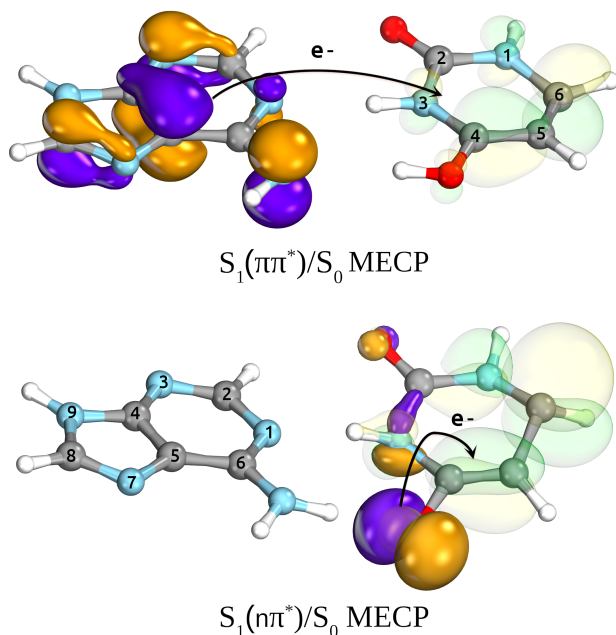


**Fig. 2** Structures of the  $^1\pi_A\pi_U^*/S_0$  and  $^1n_U\pi_U^*/S_0$  minimum energy crossing points located using SCS-MP2/SCS-ADC(2)/cc-pVTZ method for A-U. Occupied (solid purple and orange) and virtual (translucent green and yellow) molecular orbitals for the leading amplitudes are shown indicating the orbital character of the corresponding  $S_1$  state.

A comparison of  $^1\pi_A\pi_U^*/S_0$  and  $^1n_U\pi_U^*/S_0$  MECPs found on the  $S_1$  PE surface of the base pair A-U is presented in Fig. 2. The former, shown in the top panel, corresponds to the EDPT channel. The amino hydrogen transfer that follows the  $\pi_U^* \leftarrow \pi_A$  CT transition stabilizes the structure, and the most noticeable geometric changes are the elongation of the C4-O bond of U by 0.14 Å due to keto-enol tautomerization and the change in dihedral angle  $\delta(\text{H}_5\text{C}_5\text{C}_6\text{H}_6)$  by almost 20°. In the latter intramolecular  $^1n_U\pi_U^*/S_0$  conical intersection depicted in the lower panel, the WC A-U base pair undergoes local structural changes within the uracil molecule similar to those reported for  $S_1/S_0$  of isolated uracil by Matsika<sup>69</sup> or CI<sub>1</sub> and CI<sub>3</sub> conical intersections of isolated thymine reported by Perun et al.<sup>70</sup> Compared to the equilibrium geometry of the ground state (cf. Fig. 1), this MECP shows out-of-plane (oop) pyramidalization of the pyrimidine ring atoms N3 and C6 (mostly the latter, hence denoted U C6-oop). Despite some similarities, the observed structural changes in the base pair are not as pronounced as in bare nucleobases, presumably due to the stabilization provided by the complementary base.

Further investigation included linear interpolation in internal coordinates (LIIC) between three stationary points:  $S_0$  and  $S_1$  minimum energy structures, and the corresponding  $S_1/S_0$  MECPs.

The potential energy profiles of the low-lying electronic state for the canonical A-U are shown in Fig. 3. There are two competing mechanisms that can lead to internal conversion to the ground state. On the right side of the plot, the potential energy cuts along the amino N-H distance indicate a decay path through LE/CT and CT/ $S_0$  crossings via EDPT process. Although the barrier for this process exceeding 1 eV is most likely exaggerated due

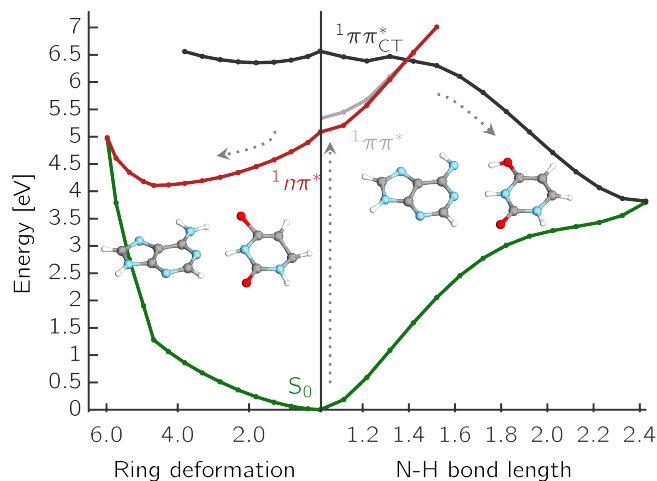


**Fig. 3** Selected mechanism of nonradiative deactivation of photoexcited A-U. The right PE cut along the amino N-H transfer shows EDPT through LE/CT and CT/ $S_0$  MECPs, while the left presents relaxation through U pucker on the  $^1n\pi^*$  PE surface with respect to the interpolated ring-puckering coordinate plotted in mass-weighted Cartesian coordinates in Å ·  $\sqrt{\text{amu}}$ .

to interpolation, the CT state is apparently inaccessible from the lowest bright states. However, considering the substantial oscillator strengths of the  $S_9$  and  $S_{11}$  states that have a leading CT  $^1\pi\pi^*$  contribution with the admixture of LE  $^1\pi\pi^*$  configurations in the FC region, they could be directly populated by UV-C pulse well below the ionization potential of the nucleobases.<sup>71,72</sup> This possibility of a direct population of the repulsive CT state could be interesting in the context of the prebiotic chemistry of nucleotides.

On the other hand, the two lowest LE states, namely the dark  $^1n\pi^*$  and bright  $^1\pi\pi^*$  are nearly degenerate along the first few steps of interpolation at the SCS-ADC(2) level, increasing the chance of internal conversion from the bright to the dark excited state of the  $^1n\pi^*$  character. Although it is generally known that the population of the  $^1n\pi^*$  state of thymine is strongly reduced in the polar solvent<sup>73</sup> and base pairing also destabilizes these transitions,<sup>74,75</sup> the presence of these low-lying and long-living states can be a significant factor in the observed relaxation impediment due to EDPT<sup>42</sup> because their population can lead to other internal conversion processes and intersystem crossing to triplet states in pyrimidines.<sup>60,62</sup> Presumably, these channels may compete or even dominate in non-radiative deactivation processes of A-T/A-U. Taking into account experimental evidence of photorelaxation through the EDPT channel in the adenine homodimer,<sup>66</sup> it is worth considering that the processes involving pyrimidines are indeed an obstacle to effective relaxation through the exchange of protons along hydrogen bonds.

The locally excited  $^1n_U\pi_U^*$  state lies 0.24 eV below the  $S_3$  bright state of a partial  $^1\pi_U\pi_U^*$  character in the FC region. Thus, after photoexcitation to the bright state, there is an opportunity to cross with the lower lying  $^1n\pi^*$  in a barrierless manner and trigger the competing deactivation mechanism presented on the left side of Fig. 3. In this scenario, the wavepacket evolves on the surface of the  $S_1$   $^1n\pi^*$  state toward the  $S_1$  PE minimum along the pyrimidine ring deformation coordinate and then to the  $S_1/S_0$  MECP.



adenine C2-N3 and C2-N1 bonds by 0.09 Å and 0.08 Å, respectively. The dihedral angle  $\delta(N_1C_2N_3C_4)$  of adenine changes from 0° to 63.4° with respect to the ground state structure. This MECF is located 4.33 eV above the ground state, which is 0.49 eV lower than the other C2-puckered MECF and is easily accessible from the FC region. The alternative higher-lying C2-puckered MECF is presented to the top right of Fig. 4. It shows a significant displacement along the C2-N3 bond of adenine (elongated by 0.17 Å) and the dihedral angle  $\delta(N_1C_2N_3C_4)$  that changed from 0° to -81.6°, with respect to the equilibrium geometry. This MECF features a slightly sloped topography; however, the energy barrier from the corresponding  $S_1$  PE minimum to  $S_1/S_0$  MECF amounts only to 0.28 eV, which is roughly a third of that found for  $^1n\pi^*/S_0$ .

We also located the C6-puckered MECF in the A-T and A-U base pairs. The corresponding structure and interpolated PE profile for A-U are shown in the left part of Fig. 4. This MECF is characterized by the elongation of the adenine N1-C6 bond by 0.13 Å and the change in the dihedral angle  $\delta(C_2N_1C_6C_5)$  from 0° to -42.2°. This MECF also features an out-of-plane distortion of the -NH<sub>2</sub> group and is the most distorted of all puckered structures, as indicated by the mass-weighted displacement of the Cartesian coordinates. The dihedral angle between the N9-C8 bond of adenine and the N1-C2 bond of uracil,  $\delta([A]N_9C_8 - N_1C_2[U])$ , changes from 0° to 88.8°. As with the previously discussed C2-puckering paths, the C6-puckering mechanism appears to be easily accessible from the FC region, although the corresponding MECF has a slightly sloped topography.

According to the findings of Jouybari et al.<sup>27</sup> we also attempted to find the photorelaxation mechanisms that may occur on the  $\pi\pi^*$  PE hypersurfaces of T and U. Unfortunately, geometry optimization leads to structures returning negative excitation energies, which indicates a multireference character of the wavefunction that is not adequately described by the SCS-ADC(2) method. Furthermore, optimization of the geometry of the  $^1n_A\pi_A^*$  excited state for A-U and A-T leads to the  $^1\pi_A\pi_A^*$  minimum, even though we were able to locate the corresponding  $^1n_A\pi_A^*$  minimum energy structure of isolated adenine. This may be a consequence of the formation of hydrogen bonds involving the N1 lone electron pair, which results in an increased energy of  $n\pi^*$  transitions.<sup>21</sup> All of this indicates that the discussed minima are inaccessible from the FC region of A-U/A-T, particularly since these states lie higher than those previously discussed (cf. Table 1).

The mechanisms discussed so far are mainly related to the WC A-U base pair and the relevant critical points are plotted schematically in Fig. 5. The results obtained for A-T are qualitatively similar and are presented in Fig. S1 of the ESI, showing the relative energies of the excited-state minima and MECFs. The differences in these data between A-U and A-T are within 0.01-0.05 eV.

The distortion of all the discussed intramolecular MECFs from the quasi-planar structure raises the question of the plausibility of these paths in DNA and RNA structures. In particular, MECFs associated with the C2- and C6-atom puckering of adenine feature a significant out-of-plane distortion. To explore whether the puckered structures are accessible in nucleic acid, we performed a search of the experimental B-DNA structures. When the structural deformations of the puckered MECFs are taken into account,

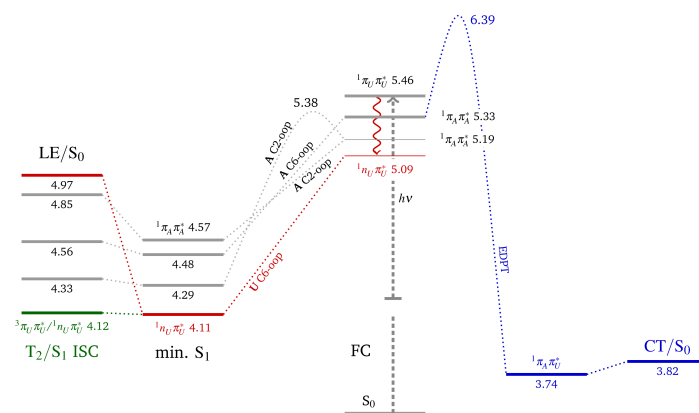


**Fig. 5** Schematic representation of the investigated radiationless deactivation mechanisms in the A-U base pair. The values show energies relative to the ground state in eV. Ring-puckering paths are labeled with puckered base and the most distorted ring atom, e.g. U C6-oop indicates uracil atom C6 distorted out of plane.

the *propeller twist* parameter seems to reflect the change in the mutual orientation of the nucleobases most reliably.<sup>88</sup>

The average value of this parameter for A-T in the experimental results collected (data gathered at 22/09/2023) from the nucleic acid database<sup>89,90</sup> is 22.9°, while the BIGNASim molecular dynamics simulations database,<sup>91</sup> employing Nucleic Acids Flexibility Server,<sup>92</sup> shows that this parameter can change up to 53.6°. The data presented pertain only to a naked B-DNA duplex with at least two A-T base pairs in a sequence. The average and extreme values of the propeller twist parameter could be compared to the values of the dihedral angle  $\delta([A]N_9C_8 - C_2N_1[U])$  which amounts to 21.8° and 5.1° for the two C2-oop(A) MECFs, and 88.8° and 31.4° for the C6-oop(A) and C6-oop(U) MECFs, respectively. Therefore, only the C6-puckered MECF geometry does not fit into these ranges and may be unattainable in the larger RNA fragment.

### 3.2 Calibration

It should be noted that initially the PE profiles were computed using the MP2 method for the ground state and the ADC(2) method for the excited states. These were further compared with the results of the spin component scaling variants<sup>93</sup> of these methods (that is, SCS-MP2 and SCS-ADC(2)), assuming the same interpolated geometries. Recent studies indicated that the SCS variant of the CC2 method essentially alleviates the underestimation of excitation energies (i.e. excessive stabilization) of CT, Rydberg and  $n\pi^*$  states.<sup>64</sup> Since the ADC(2) method suffers from similar problems, considering the formal similarities between the ADC(2) and CC2 methods, the SCS variant should produce a more balanced description of the valence and CT states.

The accuracy of the chosen methodology was tested against the results obtained using the state-averaged  $n$ -electron valence perturbation method (SA-NEVPT2) assuming the same interpolated geometries. The complete active space in NEVPT2 calculations included 10 electrons correlated in 8 orbitals (3 occupied  $\pi$ , 2 occupied  $n$  and 3 virtual  $\pi^*$ ). Such active space was reported to

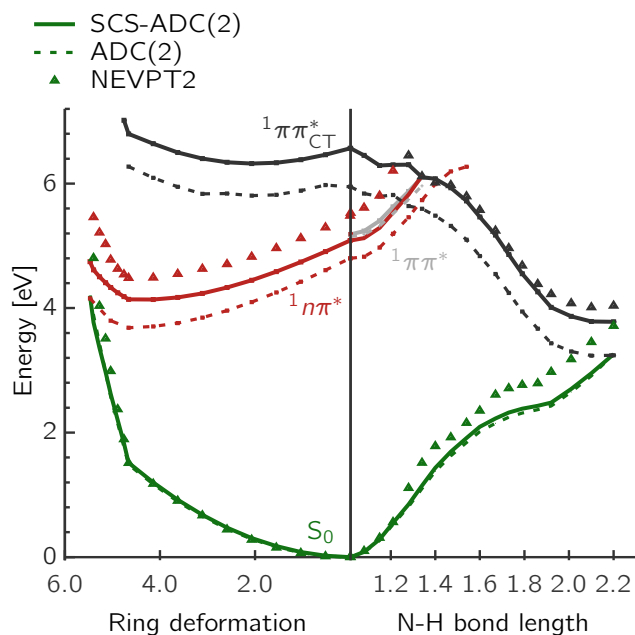


**Fig. 6** Selected mechanism of nonradiative deactivation of photoexcited A-U. On the right PE cut along the amino N-H transfer shows EDPT via LE/CT and CT/S<sub>0</sub> and on the left relaxation through U puckering on the <sup>1</sup>nπ\* surface is schematically presented with respect to the interpolated ring-puckering plotted in mass-weighted Cartesian coordinates in Å · √amu.

be correct for an appropriate description of the CT states.<sup>94</sup> It can be concluded from Fig. 6 that the SCS-ADC(2) method returns reliable energies of the <sup>1</sup>ππ\* states that agree well with the NEVPT2 results, in stark contrast to the ADC(2) approach, which systematically underestimates the energies of the <sup>1</sup>π<sub>A</sub>π<sub>A</sub> CT and <sup>1</sup>nπ\* states. The excitation energies obtained using the SCS-ADC(2) method are slightly underestimated for the <sup>1</sup>nπ\* states. It is also well documented that hydrogen bonding destabilizes the <sup>1</sup>nπ\* states in WC base pairs,<sup>21,77</sup> and their description is more demanding than the <sup>1</sup>ππ\* states.

Note that the interpolated PE profiles of the S<sub>0</sub> state calculated using different variants of the ADC(2) method (shown with solid and dashed green lines) are virtually identical. However, there is a substantial difference between the SCS-ADC(2) or NEVPT2 results and the ADC(2) results for the CT state (black lines or triangles) and the <sup>1</sup>nπ\* state (red lines), particularly in the close proximity of the conical intersection region. It shows that although the choice of the theoretical approach does not affect the description of the PE surface in the ground state, it is essential to determine the PE surfaces of the CT and <sup>1</sup>nπ\* states, and hence the MECPs with these surfaces. The SCS approach is also advantageous in the context of intermolecular interaction among nucleobases. The dispersion interaction in base pairs has been indicated to be substantially overestimated by MP2 method<sup>95,96</sup> which is to some extent corrected when the SCS-MP2 variant is used. Therefore, in the discussion, we focus on the results of SCS-MP2/SCS-ADC(2) calculations.

## 4 Conclusions

Resuming, our calculations indicate that all intramolecular channels involving either pyrimidine or purine ring distortion should be accessible from the FC region. Thus, we infer that multiple alternative relaxation pathways for A-U and A-T coexist, possibly making detection of the EDPT process more difficult in the examined systems. The latter process, even though apparently inaccessible from the lowest-lying bright state, could in principle occur after direct population of the CT state by the UV-C pulse.

The C6 and C2-puckered adenine MECPs (A C6-oop and A C2-oop) with peaked topography appear to be slightly more plausible than the C2-puckered adenine (with different ring-distortion) and the N3/C6 puckered uracil or thymine <sup>1</sup>nπ\*/S<sub>0</sub> MECPs (U/T C6-oop) with a sloped topography. The close proximity of two <sup>1</sup>π<sub>A</sub>π<sub>A</sub> bright states (shown in blue and gray lines in Fig.4) strengthens the possibility of non-radiative deactivation by puckering of adenine. Furthermore, geometric constraints within nucleic acids appear to diminish the probability of photorelaxation on the <sup>1</sup>π<sub>A</sub>π<sub>A</sub> hypersurface associated with the C6-atom puckering of adenine in the base pairs A-U and A-T in favor of the puckering of the C2 atom.

It should be underlined that experimental studies of A-T photodynamics conclude that it is dominated by intramonomer processes, involving a population of <sup>1</sup>nπ\* states.<sup>42,97</sup> Indeed, according to our calculations, there is no barrier on <sup>1</sup>nπ\* A-U PE surfaces between the FC region and the S<sub>1</sub> minimum of the <sup>1</sup>nπ\* character. The corresponding LE/S<sub>0</sub> MECPs have a strongly sloped topography with a substantial barrier of 0.86-0.87 eV. However, the near-degeneracy of the S<sub>1</sub> and T<sub>2</sub> states and the fact that they are strongly coupled through spin-orbit interaction indicate an efficient intersystem crossing, whose estimated rate of 1.6 × 10<sup>10</sup> s<sup>-1</sup>, exceeds by an order of magnitude the corresponding internal conversion to the ground state.

## 5 Acknowledgments

This work was supported by a grant no 2021/42/N/ST4/04532 from the National Science Centre Poland. The authors acknowledge the resources granted by the Wrocław Centre of Networking and Supercomputing (WCSS).

## References

- 1 C. E. Crespo-Hernández, B. Cohen, P. M. Hare and B. Kohler, *Chemical Reviews*, 2004, **104**, 1977–2020.
- 2 C. T. Middleton, K. d. L. Harpe, C. Su, Y. K. Law, C. E. Crespo-Hernández and B. Kohler, *Annual Review of Physical Chemistry*, 2009, **60**, 217–239.
- 3 K. Kleinermanns, D. Nachtigallová and M. S. de Vries, *International Reviews in Physical Chemistry*, 2013, **32**, 308–342.
- 4 M. Barbatti, A. C. Borin and S. Ullrich, *Photoinduced Phenomena in Nucleic Acids I*, Springer International Publishing, Cham, 2014, vol. 355, pp. 1–32.
- 5 A. Giussani, J. Segarra-Martí, D. Roca-Sanjuán and M. Merchán, *Photoinduced Phenomena in Nucleic Acids I: Nucleobases in the Gas Phase and in Solvents*, Springer International Publishing, Cham, 2015, pp. 57–97.

- 6 S. Mai, M. Richter, P. Marquetand and L. González, *Photoinduced Phenomena in Nucleic Acids I: Nucleobases in the Gas Phase and in Solvents*, Springer International Publishing, Cham, 2015, pp. 99–153.
- 7 R. Improta, F. Santoro and L. Blancafort, *Chemical Reviews*, 2016, **116**, 3540–3593.
- 8 L. Martinez Fernandez, F. Santoro and R. Improta, *Accounts of Chemical Research*, 2022, **55**, 2077–2087.
- 9 A. L. Sobolewski, W. Domcke and C. Hattig, *Proceedings of the National Academy of Sciences*, 2005, **102**, 17903–17906.
- 10 S. Perun, A. L. Sobolewski and W. Domcke, *The Journal of Physical Chemistry A*, 2006, **110**, 9031–9038.
- 11 G. Groenhof, L. V. Schäfer, M. Boggio-Pasqua, M. Goette, H. Grubmüller and M. A. Robb, *Journal of the American Chemical Society*, 2007, **129**, 6812–6819.
- 12 P. R. Markwick, N. L. Doltsinis and J. Schlitte, *The Journal of Chemical Physics*, 2007, **126**, 01B623.
- 13 E. Samoylova, T. Schultz, I. Hertel and W. Radloff, *Chemical Physics*, 2008, **347**, 376–382.
- 14 K. B. Bravaya, O. Kostko, M. Ahmed and A. I. Krylov, *Physical Chemistry Chemical Physics*, 2010, **12**, 2292–2307.
- 15 Y.-J. Ai, F. Zhang, G.-L. Cui, Y. Luo and W.-H. Fang, *The Journal of Chemical Physics*, 2010, **133**, 064302.
- 16 J. P. Gobbo, V. Sauri, D. Roca-Sanjuan, L. Serrano-Andres, M. Merchán and A. C. Borin, *The Journal of Physical Chemistry B*, 2012, **116**, 4089–4097.
- 17 P. G. Szalay, T. Watson, A. Perera, V. Lotrich and R. J. Bartlett, *The Journal of Physical Chemistry A*, 2013, **117**, 3149–3157.
- 18 M. K. Shukla and J. Leszczynski, *WIREs Computational Molecular Science*, 2013, **3**, 637–649.
- 19 L. Blancafort and A. A. Voityuk, *The Journal of Chemical Physics*, 2014, **140**, 095102.
- 20 Y. Zhang, K. de La Harpe, A. A. Beckstead, R. Improta and B. Kohler, *Journal of the American Chemical Society*, 2015, **137**, 7059–7062.
- 21 Z. Benda and P. G. Szalay, *Physical Chemistry Chemical Physics*, 2016, **18**, 23596–23606.
- 22 V. A. Spata, W. Lee and S. Matsika, *The Journal of Physical Chemistry Letters*, 2016, **7**, 976–984.
- 23 B. Marchetti, T. N. V. Karsili, M. N. R. Ashfold and W. Domcke, *Physical Chemistry Chemical Physics*, 2016, **18**, 20007–20027.
- 24 I. Conti and M. Garavelli, *The Journal of Physical Chemistry Letters*, 2018, **9**, 2373–2379.
- 25 K. E. Szkaradek, P. Stadlbauer, J. Šponer, R. W. Góra and R. Szabla, *Chemical Communications*, 2020, **56**, 201–204.
- 26 L. J. Karas, C.-H. Wu, H. Ottosson and J. I. Wu, *Chemical Science*, 2020, **11**, 10071–10077.
- 27 M. Y. Jouybari, J. A. Green, R. Improta and F. Santoro, *The Journal of Physical Chemistry A*, 2021, **125**, 8912–8924.
- 28 J. A. Green, M. Yaghoubi Jouybari, H. Asha, F. Santoro and R. Improta, *Journal of Chemical Theory and Computation*, 2021, **17**, 4660–4674.
- 29 S. Hartweg, M. Hochlaf, G. A. Garcia and L. Nahon, *The Journal of Physical Chemistry Letters*, 2023, **14**, 3698–3705.
- 30 T. Schultz, E. Samoylova, W. Radloff, I. V. Hertel, A. L. Sobolewski and W. Domcke, *Science*, 2004, **306**, 1765–1768.
- 31 A. Abo-Riziq, L. Grace, E. Nir, M. Kabelac, P. Hobza and M. S. De Vries, *Proceedings of the National Academy of Sciences*, 2005, **102**, 20–23.
- 32 P. R. Markwick and N. L. Doltsinis, *The Journal of Chemical Physics*, 2007, **126**, 05B603.
- 33 A. L. Sobolewski and W. Domcke, *Europhysics News*, 2006, **37**, 20–23.
- 34 R. C.-T. Chan, C. Ma, A. K.-W. Wong, C. T.-L. Chan, J. C.-L. Chow and W.-M. Kwok, *The Journal of Physical Chemistry Letters*, 2022, **13**, 302–311.
- 35 M. Dargiewicz, M. Biczysko, R. Improta and V. Barone, *Physical Chemistry Chemical Physics*, 2012, **14**, 8981–8989.
- 36 K. H. Johnson, D. M. Gray and J. C. Sutherland, *Nucleic Acids Research*, 1991, **19**, 2275–2280.
- 37 M. Pollum, L. Martinez-Fernandez and C. E. Crespo-Hernandez, *Photoinduced Phenomena in Nucleic Acids I: Nucleobases in the Gas Phase and in Solvents*, 2015, 245–327.
- 38 S. Reiter, D. Keefer and R. de Vivie-Riedle, *Journal of the American Chemical Society*, 2018, **140**, 8714–8720.
- 39 G. Villani, *Chemical Physics*, 2005, **316**, 1–8.
- 40 K. Röttger, H. J. Marroux, A. F. Chemin, E. Elsdon, T. A. Oliver, S. T. Street, A. S. Henderson, M. C. Galan, A. J. Orr-Ewing and G. M. Roberts, *The Journal of Physical Chemistry B*, 2017, **121**, 4448–4455.
- 41 M. Kratochvíl, J. Šponer and P. Hobza, *Journal of the American Chemical Society*, 2000, **122**, 3495–3499.
- 42 E. Samoylova, H. Lippert, S. Ullrich, I. V. Hertel, W. Radloff and T. Schultz, *Journal of the American Chemical Society*, 2005, **127**, 1782–1786.
- 43 C. Møller and M. S. Plesset, *Physical Review*, 1934, **46**, 618–622.
- 44 S. Grimme, *J. Chem. Phys.*, 2003, **118**, 9095–9102.
- 45 A. B. Trofimov and J. Schirmer, *Journal of Physics B: Atomic, Molecular and Optical Physics*, 1995, **28**, 2299.
- 46 A. Dreuw, A. Papapostolou and A. L. Dempwolff, *The Journal of Physical Chemistry A*, 2023.
- 47 TURBOMOLE v7.3 2018, a development of University of Karlsruhe and Forschungszentrum Karlsruhe GmbH, 1989–2007, TURBOMOLE GmbH, since 2007; available from <http://www.turbomole.com>.
- 48 T. H. Dunning, *The Journal of Chemical Physics*, 1989, **90**, 1007–1023.
- 49 B. G. Levine, J. D. Coe and T. J. Martinez, *The Journal of Physical Chemistry B*, 2008, **112**, 405–413.
- 50 F. Plasser, M. Wormit and A. Dreuw, *The Journal of Chemical Physics*, 2014, **141**, 024106.
- 51 F. Plasser, S. A. Bäßler, M. Wormit and A. Dreuw, *The Journal of Chemical Physics*, 2014, **141**, 024107.
- 52 F. Plasser, *The Journal of Chemical Physics*, 2020, **152**, 084108.
- 53 R. S. Mulliken, *The Journal of chemical physics*, 1955, **23**, 1833–1840.



- 54 Q. Peng, Y. Yi, Z. Shuai and J. Shao, *The Journal of Chemical Physics*, 2007, **126**, 114302.
- 55 Y. Niu, Q. Peng, C. Deng, X. Gao and Z. Shuai, *The Journal of Physical Chemistry A*, 2010, **114**, 7817–7831.
- 56 Z. Shuai, *Chinese Journal of Chemistry*, 2020, **38**, 1223–1232.
- 57 Y. Niu, W. Li, Q. Peng, H. Geng, Y. Yi, L. Wang, G. Nan, D. Wang and Z. Shuai, *Molecular Physics*, 2018, **116**, 1078–1090.
- 58 Y. Shao, Z. Gan, E. Epifanovsky, A. T. Gilbert, M. Wormit, J. Kussmann, A. W. Lange, A. Behn, J. Deng, X. Feng *et al.*, *Molecular Physics*, 2015, **113**, 184–215.
- 59 S. Mouret, C. Baudouin, M. Charveron, A. Favier, J. Cadet and T. Douki, *Proceedings of the National Academy of Sciences*, 2006, **103**, 13765–13770.
- 60 P. M. Hare, C. E. Crespo-Hernández and B. Kohler, *Proceedings of the National Academy of Sciences*, 2007, **104**, 435–440.
- 61 R. Szabla, H. Kruse, J. Šponer and R. W. Góra, *Physical Chemistry Chemical Physics*, 2017, **19**, 17531–17537.
- 62 A. J. Pepino, J. Segarra-Martí, A. Nenov, I. Rivalta, R. Improta and M. Garavelli, *Physical Chemistry Chemical Physics*, 2018, **20**, 6877–6890.
- 63 J. Dezalay, M. Broquier, S. Soorkia and G. Grégoire, *The European Physical Journal D*, 2021, **75**, 1–11.
- 64 A. Tajti and P. G. Szalay, *Journal of Chemical Theory and Computation*, 2019, **15**, 5523–5531.
- 65 Y. Lu, Z. Lan and W. Thiel, *Angewandte Chemie*, 2011, **123**, 6996–6999.
- 66 I. Hünig, C. Plützer, K. A. Seefeld, D. Löwenich, M. Nispel and K. Kleinermanns, *A European Journal of Chemical Physics and Physical Chemistry*, 2004, **5**, 1427–1431.
- 67 C. E. Crespo-Hernández, B. Cohen and B. Kohler, *Nature*, 2005, **436**, 1141–1144.
- 68 K. Röttger, H. J. B. Marroux, M. P. Grubb, P. M. Coulter, H. Böhnke, A. S. Henderson, M. C. Galan, F. Temps, A. J. Orr-Ewing and G. M. Roberts, *Angewandte Chemie International Edition*, 2015, **54**, 14719–14722.
- 69 S. Matsika, *The Journal of Physical Chemistry A*, 2004, **108**, 7584–7590.
- 70 S. Perun, A. L. Sobolewski and W. Domcke, *The Journal of Physical Chemistry A*, 2006, **110**, 13238–13244.
- 71 D. Roca-Sanjuán, M. Rubio, M. Merchán and L. Serrano-Andrés, *The Journal of Chemical Physics*, 2006, **125**, 084302.
- 72 K. Lewis, K. Copeland and G. Hill, *International Journal of Quantum Chemistry*, 2014, **114**, 1678–1684.
- 73 J. Cerezo, Y. Liu, N. Lin, X. Zhao, R. Improta and F. Santoro, *Journal of Chemical Theory and Computation*, 2018, **14**, 820–832.
- 74 F. Santoro, V. Barone and R. Improta, *ChemPhysChem*, 2008, **9**, 2531–2537.
- 75 F. Santoro, V. Barone and R. Improta, *Journal of the American Chemical Society*, 2009, **131**, 15232–15245.
- 76 M. Etinski, *Journal of the Serbian Chemical Society*, 2011, **76**, 1649–1660.
- 77 H. Böhnke, K. Röttger, R. A. Ingle, H. J. Marroux, M. Bohnsack, N. K. Schwalb, A. J. Orr-Ewing and F. Temps, *The Journal of Physical Chemistry B*, 2019, **123**, 2904–2914.
- 78 S. Perun, A. L. Sobolewski and W. Domcke, *Journal of the American Chemical Society*, 2005, **127**, 6257–6265.
- 79 L. Blancafort, *Journal of the American Chemical Society*, 2006, **128**, 210–219.
- 80 L. Serrano-Andres, M. Merchán and A. C. Borin, *Proceedings of the National Academy of Sciences*, 2006, **103**, 8691–8696.
- 81 L. Serrano-Andrés, M. Merchán and A. C. Borin, *Journal of the American Chemical Society*, 2008, **130**, 2473–2484.
- 82 M. Barbatti, Z. Lan, R. Crespo-Otero, J. J. Szymczak, H. Lischka and W. Thiel, *The Journal of Chemical Physics*, 2012, **137**, 22A503.
- 83 M. Barbatti and H. Lischka, *Journal of the American Chemical Society*, 2008, **130**, 6831–6839.
- 84 M. Barbatti, A. J. A. Aquino, J. J. Szymczak, D. Nachtigallová, P. Hobza and H. Lischka, *Proceedings of the National Academy of Sciences*, 2010, **107**, 21453–21458.
- 85 J. W. Park and T. Shiozaki, *Journal of Chemical Theory and Computation*, 2017, **13**, 3676–3683.
- 86 F. Plasser, R. Crespo-Otero, M. Pedersoli, J. Pittner, H. Lischka and M. Barbatti, *Journal of chemical theory and computation*, 2014, **10**, 1395–1405.
- 87 Y. Lu, Z. Lan and W. Thiel, *Journal of computational chemistry*, 2012, **33**, 1225–1235.
- 88 R. E. Dickerson, *Nucleic acids research*, 1989, **17**, 1797–1803.
- 89 H. M. Berman, W. K. Olson, D. L. Beveridge, J. Westbrook, A. Gelbin, T. Demeny, S.-H. Hsieh, A. Srinivasan and B. Schneider, *Biophysical Journal*, 1992, **63**, 751.
- 90 B. Coimbatore Narayanan, J. Westbrook, S. Ghosh, A. I. Petrov, B. Sweeney, C. L. Zirbel, N. B. Leontis and H. M. Berman, *Nucleic Acids Research*, 2014, **42**, D114–D122.
- 91 A. Hospital, P. Andrio, C. Cugnasco, L. Codo, Y. Becerra, P. D. Dans, F. Battistini, J. Torres, R. Goni, M. Orozco *et al.*, *Nucleic Acids Research*, 2016, **44**, D272–D278.
- 92 A. Hospital, I. Faustino, R. Collepardo-Guevara, C. Gonzalez, J. L. Gelpí and M. Orozco, *Nucleic Acids Research*, 2013, **41**, W47–W55.
- 93 A. Hellweg, S. A. Grün and C. Hättig, *Physical Chemistry Chemical Physics*, 2008, **10**, 4119–4127.
- 94 C. Zuluaga, V. A. Spata and S. Matsika, *Journal of Chemical Theory and Computation*, 2020, **17**, 376–387.
- 95 S. M. Cybulski and M. L. Lytle, *The Journal of Chemical Physics*, 2007, **127**, 141102–141102–4.
- 96 P. R. Horn, Y. Mao and M. Head-Gordon, *Physical Chemistry Chemical Physics*, 2016, **18**, 23067–23079.
- 97 C. Canuel, M. Mons, F. Piuze, B. Tardivel, I. Dimicoli and M. Elhanine, *The Journal of Chemical Physics*, 2005, **122**, 074316.